17. E. Rollings *et al.*, *J. Phys. Chem. Solids* **67**, 2172 (2006).
18. Materials and methods are available on *Science* Online.
19. H. Boehm, R. Setton, E. Stumpp, *Pure Appl. Chem.* **66**, 1893 (1994).
20. R. A. Greinke *et al.*, U.S. Patent 6,416,815.
21. A. D. Lueking, L. Pan, D. L. Narayanan, C. E. B. Clifford, *J. Phys. Chem. B* **109**, 12710 (2005).
22. A. Star *et al.*, *Angew. Chem. Int. Ed.* **40**, 1721 (2001).
23. X. L. Li *et al.*, *J. Am. Chem. Soc.* **129**, 4890 (2007).
24. A. Javey, J. Guo, Q. Wang, M. Lundstrom, H. Dai, *Nature* **424**, 654 (2003).
25. Y. Ouyang, Y. Yoon, J. Guo, *IEEE Trans. Electron. Dev.* **54**, 2223 (2007).
26. S. Ilani, L. A. K. Donev, M. Kindermann, P. L. McEuen, *Nat. Phys.* **2**, 687 (2006).
27. R. Tu, L. Zhang, Y. Nishi, H. Dai, *Nano Lett.* **7**, 1561 (2007).
28. Y. Yoon, J. Guo, *Appl. Phys. Lett.* **91**, 073103 (2007).
29. We thank Graftech for providing the samples. This work was supported by Microelectronics Advanced Research Corporation Materials, Structures, and Devices Focus Center (MARCO MSD) and Intel.

Supporting Online Material
www.sciencemag.org/cgi/content/full/1150878/DC1
Materials and Methods
Figs. S1 to S7
References

24 September 2007; accepted 10 January 2008
Published online 24 January 2008;
10.1126/science.1150878
Include this information when citing this paper.

Deeply Inverted Electron-Hole Recombination in a Luminescent Antibody-Stilbene Complex

Erik W. Debler,[1,2]* Gunnar F. Kaufmann,[2,3,4] Michael M. Meijler,[2,3]† Andreas Heine,[1]‡ Jenny M. Mee,[2,3] Goran Pljevaljčić,[1] Angel J. Di Bilio,[5] Peter G. Schultz,[2,3] David P. Millar,[1] Kim D. Janda,[2,3,4,6] Ian A. Wilson,[1,2] Harry B. Gray,[5]§ Richard A. Lerner[1,2,3]§

The blue-emissive antibody EP2-19G2 that has been elicited against *trans*-stilbene has unprecedented ability to produce bright luminescence and has been used as a biosensor in various applications. We show that the prolonged luminescence is not stilbene fluorescence. Instead, the emissive species is a charge-transfer excited complex of an anionic stilbene and a cationic, parallel π-stacked tryptophan. Upon charge recombination, this complex generates exceptionally bright blue light. Complex formation is enabled by a deeply penetrating ligand-binding pocket, which in turn results from a noncanonical interface between the two variable domains of the antibody.

An excited-state complex (exciplex) formed by the interaction of an electronically excited molecule with a ground-state partner features charge transfer to a various extent and typically exhibits structureless emission that is red-shifted from the emissive features of its individual components (*1*, *2*). Among the rare examples of exciplex-like behavior in proteins (*3*) is the conjugate of monoclonal antibody EP2-19G2 with the *trans*-stilbene hapten **1** (Scheme 1), which emits intense blue light upon ultraviolet (UV) excitation (movie S1) (*4*).

In striking contrast to this highly luminescent complex, electronically excited *trans*-stilbene is only weakly fluorescent in solution, owing to efficient nonradiative decay via cis-trans isomerization (*5*). Unlike other antibody-stilbene complexes (*4*, *6*), the radiative lifetime of EP2-19G2-**1** is increased by more than two orders of magnitude with respect to free **1**, which substantially exceeds those of stilbene exciplexes formed with small organic molecules (*7*). From extensive examination of the structures and photophysical properties of several antibody-**1** conjugates, we have concluded that the bright blue-emissive species is a tryptophan:stilbene charge-transfer excited complex that undergoes deeply inverted electron-hole recombination in a rigid protein matrix.

Guided by the crystal structure of EP2-19G2-**1** (*4*), we identified seven antibody residues in van der Waals' contact with the stilbene aromatic system. These seven residues were then conservatively mutated and the corresponding proteins were expressed as single-chain variable antibody fragments (scFv) (*8*, *9*). Spectroscopic measurements indicated that mutation of Trp^{H103} to Phe (Trp^{H103}Phe) and Tyr^{L34} to Phe (Tyr^{L34}Phe) markedly reduced antibody-**1** emissions when compared to scFv wild-type (wt)-**1** [Fig. 1B and fig. S1 (*9*)]. As observed in the crystal structure of the EP2-19G2-**1** complex, the indole ring of Trp^{H103} is π-stacked parallel to the deeply buried phenyl ring of the stilbene ligand at an inter-

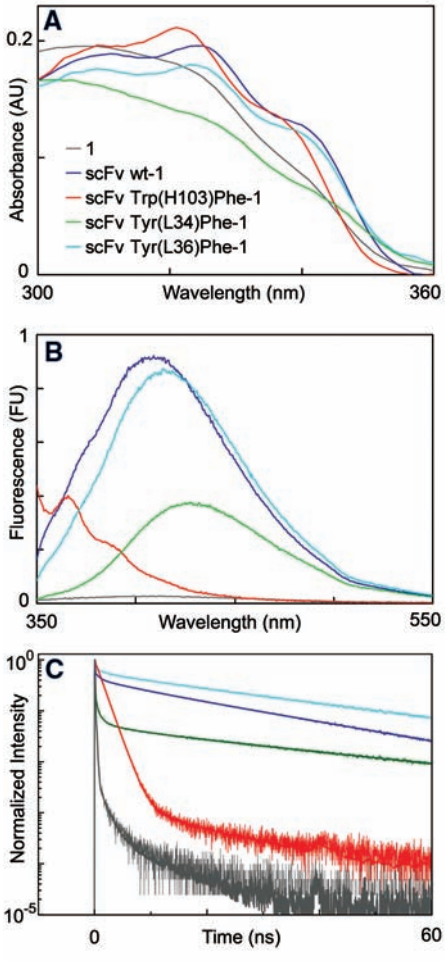

Fig. 1. (**A**) Steady-state absorption spectra of **1** (10 μM) and antibody-**1** complexes (10 μM) in PBS containing 3% DMF at room temperature. (**B**) Steady-state emission spectra of **1** (20 nM) and antibody-**1** complexes (20 nM) in PBS containing 3% DMF at room temperature. Antibody was used in large excess to ensure that the dye was completely bound by protein. (**C**) Time-resolved emission decay profiles of antibody-**1** complexes (3 μM) obtained with picosecond excitation at 303 nm. Decays were measured by time-correlated single-photon counting. Decays were recorded in 4096 channels with a time increment of 22 ps/channel and were normalized relative to the number of counts recorded in the peak channel.

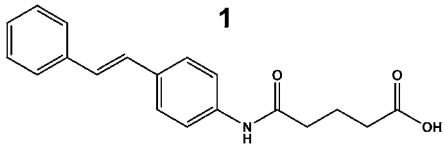

Scheme 1.

[1]Department of Molecular Biology, The Scripps Research Institute, La Jolla, CA 92037, USA. [2]The Skaggs Institute for Chemical Biology, The Scripps Research Institute, La Jolla, CA 92037, USA. [3]Department of Chemistry, The Scripps Research Institute, La Jolla, CA 92037, USA. [4]Department of Immunology, The Scripps Research Institute, La Jolla, CA 92037, USA. [5]Beckman Institute, California Institute of Technology, Pasadena, CA 91125, USA. [6]Worm Institute of Research and Medicine, The Scripps Research Institute, La Jolla, CA 92037, USA.

*Present address: Laboratory of Cell Biology, The Rockefeller University, New York, NY 10065, USA.
†Present address: Department of Chemistry, Ben-Gurion University of the Negev, Israel.
‡Present address: Institute of Pharmaceutical Chemistry, Philipps-University Marburg, 35032 Marburg, Germany.
§To whom correspondence should be addressed. E-mail: rlerner@scripps.edu (R.A.L.); hbgray@caltech.edu (H.B.G.)

planar distance of 3.5 Å, whereas the Tyr^{L34} phenoxyl group is roughly perpendicular to the stilbene molecule, pointing toward its central double bond. Thus, we focused on these two residues, with the wild-type and Tyr^{L36}Phe mutant scFv fragments acting as controls. To exclude the possibility that the much weaker emission is the result of vastly diminished binding, we confirmed that mutant scFv constructs still bind tightly to hapten **1** (Table 1) (*9*).

The absorption spectra of Trp^{H103}Phe-**1** and Tyr^{L36}Phe-**1** closely resemble that of wt-**1**, featuring well-resolved, vibronic features (Fig. 1A). By contrast, the corresponding absorption system of Tyr^{L34}Phe-**1** is less structured and similar to that of free **1** in solution. The highly structured absorption system suggests that stilbene is in a constrained environment within the binding pockets of the Trp^{H103}Phe and Tyr^{L36}Phe mutants, whereas it appears to be less restricted in the Tyr^{L34}Phe protein, consistent with its decreased affinity and fluorescence anisotropy (Table 1).

The Tyr^{L34}Phe-**1** complex exhibits less intense, red-shifted emission compared with that of wt-**1** (Fig. 1B). By contrast, the emission spectrum of Trp^{H103}Phe-**1** differs markedly from that of wt-**1**, with a large blue-shift (λ_{max} at 366 nm) and even lower intensity (0.12 quantum yield) than observed for the Tyr^{L34}Phe-**1** (0.23), with a vibronically structured shoulder on the low-energy side. For comparison, both wt-**1** and Tyr^{L36}Phe-**1** emit much more intensely, with quantum yields of 0.57 and 0.55, respectively (Table 1). Notably, the scFv wt-**1** emission quantum yield is lower than that of Fab (fragment antigen binding) wt-**1** (0.71) and is most likely attributable to a less rigid binding pocket in the single-chain construct, an interpretation that also is consistent with its lower affinity for the hapten (Table 1).

Our steady-state emission measurements show clearly that the Trp^{H103} mutation greatly enhances nonradiative decay of electronically excited EP2-19G2-**1**. By using picosecond, time-resolved emission spectroscopy, we found that the long component (>20 ns) of the multi-exponential luminescence decay is essentially abolished (amplitude <0.1%) in Trp^{H103}Phe-**1** (Fig. 1C and table S1); this component, which is a major feature in the radiative decay of both wt-**1** (17%) and Tyr^{L36}Phe-**1** (27%), is also reduced substantially in Tyr^{L34}Phe-**1** (2%) (Table 1). Because of the presence of a long decay time, greatly exceeding the radiative lifetime of **1** itself, we suggest that a Trp:stilbene charge-transfer excited complex is responsible for the slow emissive decay component.

Trp^{H103} is a highly conserved framework residue of the immunoglobulin fold and, owing to its deep burial within the variable domain, rarely interacts with antigens. However, the Trp^{H103} indole closely associates with the "distal" phenyl ring of **1** in the EP2-19G2-**1** complex. If this Trp:stilbene constellation were, indeed, unique to the blue-luminescent antibody EP2-19G2-**1**, we would expect a different ligand interaction with Trp^{H103} in purple- and blue-purple–fluorescent antibodies obtained from the same immunizations with hapten **1** (*4*).

To test this hypothesis, we determined the crystal structure of the purple-fluorescent complex of Fab EP2-25C10 with **1** to 2.5 Å resolution (table S2). EP2-25C10-**1** has an emission maximum at 380 nm with a quantum yield of 0.27 and an average lifetime of 4.9 ns (*4*). The high quantum yield with respect to free stilbene most likely means that excited-state cis-trans isomerization is disfavored in the complex because the crystal structure shows that the stilbene molecule is bound in a cavity of high shape complementarity (Fig. 2A).

Table 1. Spectral data and affinities of antibody-**1** complexes and hapten **1**. All measurements were made in phosphate-buffered saline (PBS) [10 mM sodium phosphate, 150 mM NaCl (pH 7.4)] and 3% dimethyl formamide (DMF) cosolvent, at 20°C (*9*). Quinine bisulfate in 0.5 M H_2SO_4 was used as a quantum yield reference with Φ_f = 0.546 (*29*). The anisotropy r is defined as $r = (I_{||} - I_{\perp})/(I_{||} + 2I_{\perp})$, where $I_{||}$ and $I_{\perp}$ are the emission intensities measured parallel and perpendicular to the vertical excitation polarization plane. The total emission intensity after pulsed excitation was fit by the multi-exponential function $I(t) = S\Sigma_i\ \alpha_i \exp(-t/\tau_i)$, convoluted with the instrument response function, where S, α_i, and τ_i are the overall scaling factor, decay amplitude, and decay time of component i (*9*). The long component 1 of the emission decay (>20 ns) is essentially abolished (amplitude α_1 of less than 0.1%) in the Trp^{H103}Phe mutant, and the relatively high anisotropy of free **1** reflects the limited depolarization that can occur during the very short lifetime of the excited state. λ_{abs} and λ_{em}, wavelength of absorption and emission maxima, respectively; K_d, dissociation constant; NA, not applicable.

Complex	λ_{abs} (nm)	λ_{em} (nm)	Φ_f	r	α_1	τ_1 (ns)	K_d (μM)
scFv wt-**1**	324	409	0.57	0.20	0.173	22.7	1.7
scFv Tyr^{L34}Phe-**1**	303	429	0.23	0.14	0.0219	34.5	3.9
scFv Tyr^{L36}Phe-**1**	323	416	0.55	0.19	0.247	30.3	2.0
scFv Trp^{H103}Phe-**1**	328	366	0.12	0.21	0.0009	15.6	2.0
Fab wt-**1**	325	409	0.71	0.23	0.330	22.8	0.3
1	307	385	0.02	0.31	1	0.0502	NA

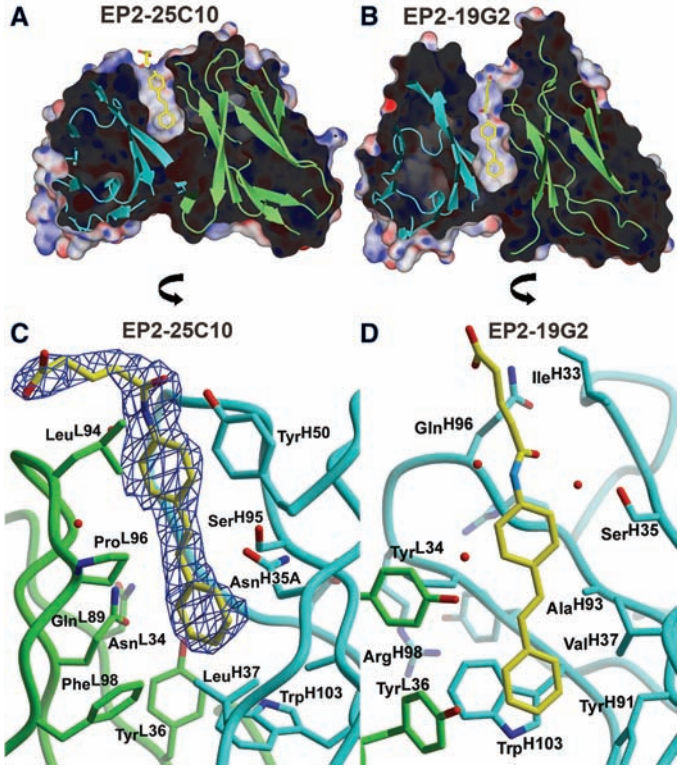

Fig. 2. Electrostatic and shape complementarity of the hapten **1** in (**A**) the EP2-25C10 and (**B**) the EP2-19G2 antibody-combining site. Slices through the center of the binding sites are shown. The heavy and light chains are colored in blue and green, respectively. The electrostatic potential was calculated in APBS (*30*) and mapped onto the surface with the color code ranging from −30 kT/e (bright red) to +30 kT/e (dark blue). Both binding pockets are highly apolar, but strongly differ in their depth and penetration of the variable antibody domain. (**C**) Crystal structure of purple-fluorescent antibody EP2-25C10 in complex with **1** (yellow). The $2F_o - F_c$ electron density map around hapten **1** is contoured at 1.5σ. (**D**) Crystal structure of the blue-emissive antibody EP2-19G2 in complex with **1** (yellow) (*4*). Trp^{H103} undergoes parallel π-stacking with **1** and forms a charge-transfer complex in the excited state. In contrast, stilbene **1** in EP2-25C10 does not engage in any π-stacking interactions with tryptophan.

The binding pocket of purple-fluorescent EP2-25C10 (Fig. 2A) is as highly hydrophobic as that of blue-luminescent EP2-19G2 (Fig. 2B), suggesting that polarity effects do not account for the 30-nm blue shift in its emission maximum. However, the overall position of the stilbene ligand within the variable part of the antibody is appreciably different in these two antibodies; in EP2-25C10, the stilbene is translated by 6 Å toward the protein surface and does not penetrate the antibody-combining site as deeply as in the EP2-19G2 complex (Fig. 2, A and B).

Consequently, the deep-seated Trp^{H103} interacts minimally with stilbene in the purple-fluorescent antibody, consistent with the relatively high emission energy. Furthermore, no EP2-25C10 tryptophan residue is involved in face-to-face or face-to-edge π-stacking interactions with stilbene (Fig. 2C). The crystal structure of the green-fluorescent antibody 11G10 in complex with a donor-acceptor–substituted stilbene reveals a binding mode similar to that in EP2-25C10 (*6*), providing strong evidence that the parallel π-stacking interaction of **1** with Trp^{H103} is attributable to the unusually deep burial of stilbene in the EP2-19G2 binding cavity.

Further structural analysis revealed that the side-chain conformation of Trp^{H103} is unusual in EP2-19G2, whereas Trp^{H103} of EP2-25C10 corresponds to the canonical rotamer that is prevalent in most antibody structures at this position (Fig. 3B). However, superimposition of the variable domains of EP2-19G2, based on the conserved framework regions, with more than 20 other antibodies, including EP2-25C10 and 11G10, yielded large root-mean-square deviations (greater than 2.0 Å) (Fig. 3A) and revealed a relatively rare disposition of heavy- and light-chain variable (V_H and V_L) domains with respect to each other in this antibody (Fig. 3C). In contrast, the individual EP2-19G2 V_H and V_L domains superimpose well onto their counterparts in other antibodies.

The geometry of the V_H/V_L interface in antibodies is generally highly conserved through invariance of ~15 side chains (*10*, *11*). Examination of the V_H/V_L interface of EP2-19G2 uncovered several notable deviations from the canonical interface and revealed factors that may synergistically contribute to the unusual relative configuration of V_H and V_L. Large deviations in the backbone conformations of the complementarity determining regions (CDRs) H3 and L3 are introduced by Pro^{H101} and Pro^{L96}, respectively (Fig. 3C). Pro^{L96} leads to a considerable displacement of conserved framework residue Trp^{H47} which, in turn, propagates this perturbation to neighboring residues and strands in V_H (Fig. 3C). The base of V_H and V_L also undergoes substantial rearrangements that include Ser^{L43} and Gln^{H105}. The latter residue now points toward V_L, unlike that in all other superimposed antibody structures. Bulky side chains at the base of CDR L1 and at the beginning of the subsequent framework region (e.g., Tyr^{L34} and Tyr^{L36}) also rearrange considerably. Thus, substantial variations at the conserved V_H/V_L interface provide a structural framework for the unusual mode of ligand recognition in EP2-19G2 that is responsible for the Trp:stilbene photophysics in the antibody-**1** complex.

Why, then, is the luminescence of EP2-19G2-**1** so intense? Consider steps 1 to 3 in the following scheme (see also Fig. 4), where TrpH represents the Trp^{H103} indole side chain carrying the N-H ring proton and *hν* is the photon energy:

1. [**1**/TrpH] + *hν* → [**1***/TrpH]
2. [**1***/TrpH] → [$\mathbf{1}^{\bullet-}$/$TrpH^{\bullet+}$]*
3. [$\mathbf{1}^{\bullet-}$/$TrpH^{\bullet+}$]* → [**1**/TrpH] + *hν′*

In the first step, **1** absorbs a photon upon ultraviolet (UV) illumination. Because the singlet excited state of stilbene is a strong electron acceptor (*12*–*14*), an electron is transferred very rapidly from Trp^{H103} to **1*** to form a charge-transfer excited complex (step 2). Conversion of singlet-excited stilbene to the charge-transfer state does not occur at low temperatures, as only stilbene fluorescence is seen below 240 K (*4*). Owing to their close parallel interaction, the two aromatic rings in this charge-transfer state are tightly bound, which greatly disfavors nonradiative decay, because coupling of this deep and narrow excited well to the ground-state potential energy surface would be very weak (Fig. 4). As a result, radiationless deactivation would be expected to be much slower than radiative decay, hence giving rise to the exceptionally bright blue emission (step 3). Because the driving force for charge recombination is much greater than a reasonable estimate of the reorganization energy, and its rate is orders of magnitude lower than predicted for coupling-limited electron tunneling over a short distance in a folded polypeptide, we conclude that the intense luminescence is attributable to deeply inverted electron transfer (*15*, *16*).

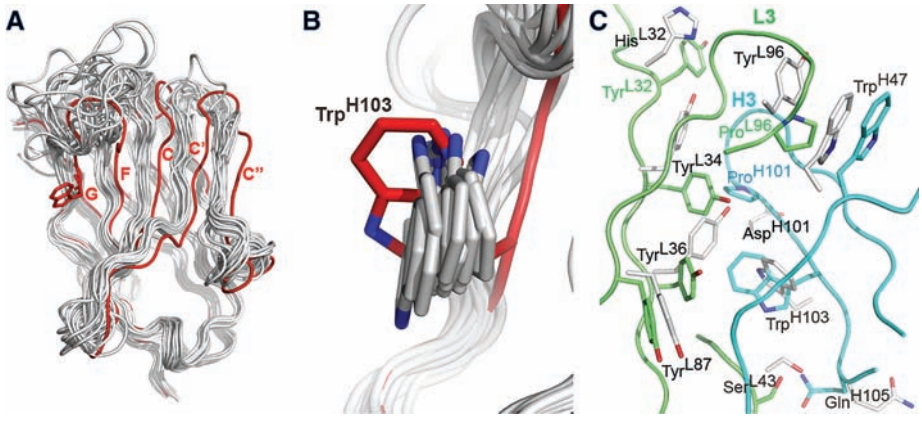

Fig. 3. (**A**) Superimposition of the EP2-19G2 variable chains (V_H + V_L domains) (red) onto other 20 catalytic antibodies (gray) based on framework regions. Only the V_H domains are shown. Trp^{H103} of EP2-19G2 is represented as a red stick. The β strands of one β sheet are labeled according to convention and clearly deviate from the corresponding strands in other antibodies. (**B**) The highly conserved Trp^{H103} features an unusual rotamer in antibody EP2-19G2 with respect to the indole side chains in the other antibodies. (**C**) Key residues at the V_H/V_L interface of EP2-19G2 (blue and green) and of a representative canonical antibody (in this case, Diels-Alder catalytic antibody 13G5, PDB ID code 1A3L, gray). Considerable structural displacements and reorientations occur over the entire interface. For clarity, some regions of EP2-19G2, as well as the backbone of 13G5, were omitted and not all conserved contacts, such as the bidentate hydrogen bond between Gln^{H39} and Gln^{L38}, are displayed. The CDRs H3 and L3 are labeled.

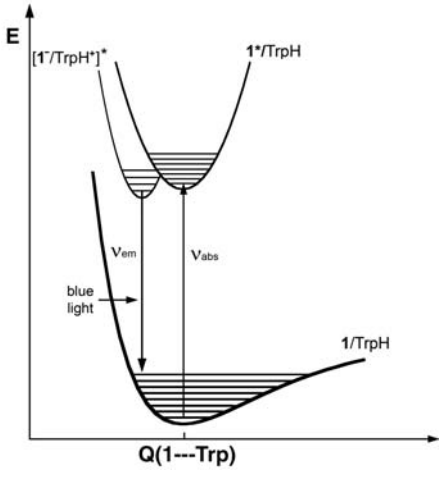

Fig. 4. Ground- and excited-state potential surfaces for EP2-19G2-**1**. After UV excitation of **1** (step 1), the stilbene excited singlet oxidizes Trp^{H103} to produce the charge-transfer complex (step 2); the interplanar distance *Q* between the cation radical Trp^{H103} and the stilbene anion **1** is shorter than in the ground state, owing to strong electrostatic binding in the hydrophobic protein cavity. In step 3, the excited charge-transfer complex returns to the ground state via electron-hole recombination that generates bright blue light in the rigid site. Radiative decay in the purple-fluorescent antibody EP2-25C10 occurs from the stilbene singlet excited state.

In view of this light-generating mechanism, the "blue-fluorescent antibody" EP2-19G2 should really be called a "blue-emissive" or "blue-luminescent" antibody.

Because roughly 3 eV of photon energy is stored in the charge-transfer excited state, it is predicted to be both a powerful reductant and oxidant. We examined the redox activity of the charge-transfer state in experiments in which irradiation of EP2-19G2-**1** was followed by flash-freezing, yielding a weak electron paramagnetic resonance signal that is attributable to a neutral tyrosyl radical having a small dihedral angle [fig. S2 (*9*)] (*17*). We suggest that a relatively small population of charge-transfer states decays by electron transfer from a tyrosine to the tryptophan radical cation, a proposal that is supported by our finding that the addition of an electron acceptor, namely $[Co(NH_3)_5Cl]^{2+}$, greatly enhances the radical signal (*17*). It is likely that the stilbene anion radical in the charge-transfer state would be oxidized rapidly by Co(III), leaving the Trp cation radical without its electron-transfer partner. The flash-quench–generated [**1**/$TrpH^{\bullet+}$] cation would then have time to oxidize any nearby protein residue, and our experiments show that tyrosine is the main electron donor.

Charge separation and recombination between a chromophore and tryptophan or tyrosine have been investigated previously in other systems (*18*–*21*). Very efficient fluorescence quenching is observed in most cases. Notably, the loss of fluorescence is due to very rapid charge recombination following femtosecond electron transfer between riboflavin and a parallel, π-stacked tryptophan after electronic excitation of the riboflavin-binding protein (*18*). Similarly, the strong fluorescence of fluorescein is quenched upon binding to antibody 4-4-20 via electron transfer from a parallel, π-stacked tyrosine in the antibody-combining site (*19*, *20*); further, the fluorescence of an anticalin-fluorescein complex is efficiently quenched by rapid electron transfer from either a coplanar tryptophan or tyrosine to singlet excited fluorescein (*21*). We conclude that the very bright blue luminescence of EP2-19G2-**1** is attributable to electron-hole recombination of the Trp:stilbene charge-transfer excited state held in the rigid EP2-19G2 matrix that disfavors nonradiative decay.

Protein luminescence (*22*) only rarely (if ever) occurs by electron-hole recombination in a charge-transfer excited state embedded in a polypeptide matrix. The distinctive photophysical properties of the antibody-stilbene complex have already been exploited in chiral sensing for high-throughput screening for the evaluation of catalysts in asymmetric synthesis (*23*, *24*), sensing mercury (*25*), DNA hybridization assays (*26*, *27*), and for analysis of accessible cysteine residues on viral surfaces (*28*). The programmed generation of antibodies against other chromophores may yield novel protein-ligand systems with similar charge recombination-induced luminescence phenomena and further biosensor applications.

References and Notes

1. J. B. Birks, *Photophysics of Aromatic Molecules* (Wiley, New York, 1970), pp. 420–421.
2. N. J. Turro, *Modern Molecular Photochemistry* (University Science Books, Mill Valley, CA, 1991), pp. 137–146.
3. A. Murza *et al*., *Biochemistry* **39**, 10557 (2000).
4. A. Simeonov *et al*., *Science* **290**, 307 (2000).
5. J. Saltiel, J. L. Charlton, in *Rearrangements in Ground and Excited States*, P. de Mayo, Ed. (Academic Press, New York, 1980), vol. 42, pp. 25–89.
6. F. Tian *et al*., *Angew. Chem. Int. Ed.* **45**, 7763 (2006).
7. F. D. Lewis, *Acc. Chem. Res.* **12**, 152 (1979).
8. Heavy-chain mutants: Ser(H35)Ala, Val(H37)Leu, Tyr(H91)Phe, Trp(H103)Phe; light-chain mutants: Tyr(L34)Phe, Tyr(L36)Phe, Phe(L98)Tyr, Tyr(L34)Phe/Phe(L98)Tyr.
9. Details for the preparation of the scFv mutants and for the biophysical characterization are available as supporting material on *Science* Online.
10. C. Chothia, J. Novotny, R. Bruccoleri, M. Karplus, *J. Mol. Biol.* **186**, 651 (1985).
11. J. Novotny, E. Haber, *Proc. Natl. Acad. Sci. U.S.A.* **82**, 4592 (1985).
12. The glutaric amide group of **1** minimally perturbs the electronic structure of *trans*-stilbene (*4*). Thus, we estimate the reduction potential of **1** to be −1.9 V versus the normal hydrogen electrode (NHE) (*13*), and that of **1*** to be about +1.4 V versus NHE. The Trp cation radical reduction potential is estimated to be +1.1 V versus NHE (*14*).
13. R. S. Ruoff, K. M. Kadish, P. Boulas, E. C. M. Chen, *J. Phys. Chem.* **99**, 8843 (1995).
14. C. Tommos, J. J. Skalicky, D. L. Pilloud, A. J. Wand, P. L. Dutton, *Biochemistry* **38**, 9495 (1999).
15. H. B. Gray, J. R. Winkler, *Annu. Rev. Biochem.* **65**, 537 (1996).
16. H. B. Gray, J. R. Winkler, *Q. Rev. Biophys.* **36**, 341 (2003).
17. A. J. Di Bilio *et al*., *J. Am. Chem. Soc.* **123**, 3181 (2001).
18. D. Zhong, A. H. Zewail, *Proc. Natl. Acad. Sci. U.S.A.* **98**, 11867 (2001).
19. M. Whitlow, A. J. Howard, J. F. Wood, E. W. Voss Jr., K. D. Hardman, *Protein Eng.* **8**, 749 (1995).
20. L. K. Denzin, G. A. Gulliver, E. W. Voss Jr., *Mol. Immunol.* **30**, 1331 (1993).
21. M. Götz, S. Hess, G. Beste, A. Skerra, M. E. Michel-Beyerle, *Biochemistry* **41**, 4156 (2002).
22. N. C. Shaner, P. A. Steinbach, R. Y. Tsien, *Nat. Methods* **2**, 905 (2005).
23. M. Matsushita *et al*., *Angew. Chem. Int. Ed.* **42**, 5984 (2003).
24. H. Matsushita *et al*., *Mol. Biosyst.* **1**, 303 (2005).
25. M. Matsushita, M. M. Meijler, P. Wirsching, R. A. Lerner, K. D. Janda, *Org. Lett.* **7**, 4943 (2005).
26. D. W. Chen *et al*., *J. Org. Chem.* **66**, 1725 (2001).
27. G. F. Kaufmann *et al*., *Angew. Chem. Int. Ed.* **44**, 2144 (2005).
28. Q. Wang, K. S. Raja, K. D. Janda, T. W. Lin, M. G. Finn, *Bioconjug. Chem.* **14**, 38 (2003).
29. G. A. Crosby, J. N. Demas, *J. Phys. Chem.* **75**, 991 (1971).
30. N. A. Baker, D. Sept, S. Joseph, M. J. Holst, J. A. McCammon, *Proc. Natl. Acad. Sci. U.S.A.* **98**, 10037 (2001).

31. We thank S. Ferguson for assistance in Fab preparation and the staff at Advanced Light Source beamline 5.0.1 for their support. We gratefully acknowledge A. Deniz for providing access to his fluorimeter, and S. Mukhopadhyay for assistance with anisotropy measurements as well as helpful discussions. We thank J. Saltiel as well as the reviewers for critically reading the manuscript and providing helpful comments. Coordinates and structure factors for the EP2-25C10-**1** complex have been deposited at the Protein Data Bank (PDB) with accession number 2NZR. Supported by NIH grants GM38273 (I.A.W.), GM56528 (P.G.S.), and DK19038 (H.B.G.) and a Skaggs predoctoral fellowship and Jairo H. Arévalo fellowship from The Scripps Research Institute graduate program (E.W.D.). This is publication 18959-MB from The Scripps Research Institute.

Supporting Online Material

www.sciencemag.org/cgi/content/full/319/5867/1232/DC1
Materials and Methods
Figs. S1 to S3
Tables S1 and S2
References
Movie S1

27 November 2007; accepted 18 January 2008
10.1126/science.1153445

Land Clearing and the Biofuel Carbon Debt

Joseph Fargione,[1] Jason Hill,[2,3] David Tilman,[2]* Stephen Polasky,[2,3] Peter Hawthorne[2]

Increasing energy use, climate change, and carbon dioxide (CO_2) emissions from fossil fuels make switching to low-carbon fuels a high priority. Biofuels are a potential low-carbon energy source, but whether biofuels offer carbon savings depends on how they are produced. Converting rainforests, peatlands, savannas, or grasslands to produce food crop–based biofuels in Brazil, Southeast Asia, and the United States creates a "biofuel carbon debt" by releasing 17 to 420 times more CO_2 than the annual greenhouse gas (GHG) reductions that these biofuels would provide by displacing fossil fuels. In contrast, biofuels made from waste biomass or from biomass grown on degraded and abandoned agricultural lands planted with perennials incur little or no carbon debt and can offer immediate and sustained GHG advantages.

Demand for alternatives to petroleum is increasing the production of biofuels from food crops such as corn, sugarcane, soybeans, and palms. As a result, land in undisturbed ecosystems, especially in the Americas and Southeast Asia, is being converted to biofuel production as well as to crop production when existing agricultural land is diverted to biofuel production. Such land clearing may be further accelerated by lignocellulosic biofuels,

Deeply Inverted Electron-Hole Recombination in a Luminescent Antibody-Stilbene Complex

Erik W. Debler *et al.*

Science **319**, 1232 (2008);
DOI: 10.1126/science.1153445